Title

Decoupling electron and phonon transport in single-nanowire hybrid materials for high-performance thermoelectrics

Journal

Science Advances, 7(20)

ISSN

2375-2548

Authors

Yang, Lin
Gordon, Madeleine P
Menon, Akanksha K
et al.

Publication Date

2021-05-14

DOI

10.1126/sciadv.abe6000

Peer reviewed

MATERIALS SCIENCE

Decoupling electron and phonon transport in single-nanowire hybrid materials for high-performance thermoelectrics

Lin Yang[1†], Madeleine P. Gordon[2,3†], Akanksha K. Menon[1], Alexandra Bruefach[4,5], Kyle Haas[2,6], M. C. Scott[4,5], Ravi S. Prasher[1,7]*, Jeffrey J. Urban[2]*

Organic-inorganic hybrids have recently emerged as a class of high-performing thermoelectric materials that are lightweight and mechanically flexible. However, the fundamental electrical and thermal transport in these materials has remained elusive due to the heterogeneity of bulk, polycrystalline, thin films reported thus far. Here, we systematically investigate a model hybrid comprising a single core/shell nanowire of Te-PEDOT:PSS. We show that as the nanowire diameter is reduced, the electrical conductivity increases and the thermal conductivity decreases, while the Seebeck coefficient remains nearly constant—this collectively results in a figure of merit, *ZT*, of 0.54 at 400 K. The origin of the decoupling of charge and heat transport lies in the fact that electrical transport occurs through the organic shell, while thermal transport is driven by the inorganic core. This study establishes design principles for high-performing thermoelectrics that leverage the unique interactions occurring at the interfaces of hybrid nanowires.

INTRODUCTION

Organic semiconductors and organic-inorganic hybrid materials have garnered substantial interest for thermoelectric applications owing to their unique advantages over inorganic materials. For example, organic semiconductors can realize flexible and lightweight energy generation or heating-cooling devices with conformal geometries, and their solution processability enables the use of inexpensive and scalable manufacturing processes (*1*–*4*). This has led to a surge of interest in various applications, such as implantable medical devices (*5*), wearables for personal electronics (*6*), and Internet of Things (*3*, *7*). For a given temperature T, the efficiency of a thermoelectric material is characterized using a dimensionless figure of merit, $ZT = S^2\sigma T/\kappa$, which encompasses three material properties: Seebeck coefficient S, electrical conductivity σ, and thermal conductivity κ. Unfortunately, the well-known interdependence between σ, κ, and S in a single-phase material often complicates efforts to develop effective strategies to achieve a high ZT (*1*, *8*).

Previous efforts to enhance ZT can be broadly divided into two groups: (i) enhancing power factor through electronic doping (*8*), quantum confinement effects (*9*), etc.; and (ii) decoupling interdependence among electrical conductivity, Seebeck coefficient, and thermal conductivity through nanostructuring (*10*), hierarchical architectures (*11*), etc. However, maximizing ZT using either approach results in a compromise between σ, κ, and S in a single-phase material. For instance, among conducting polymers, poly(3,4-ethylenedioxythiophene):poly(styrenesulfonic acid) (PEDOT:PSS) is appealing because of its high electrical conductivity upon secondary doping, but a low Seebeck coefficient largely limits its thermoelectric power factor (*1*, *3*). To circumvent this challenge, efforts have been made to integrate the high σ of PEDOT:PSS with tellurium (Te) nanostructures to form hybrid core-shell systems (Te-PEDOT:PSS) that demonstrate high power factors (PF = $S^2\sigma$), while maintaining solution processability (*12*–*14*). This hybrid material system, combining organic and inorganic phases, yields thermoelectric PF exceeding that of either constituent material owing to nonlinear interactions that occur at the hard-soft interface (*12*–*14*), which results in a ZT value of ~0.1 at 300 K (*12*), and a higher ZT value of 0.39 is achieved after chemical treatment with sulfuric acid (*15*). One example of such an interaction is the better ordering of PEDOT domains upon introduction of Te nanowires, which has been theoretically shown to improve the electrical conduction in the organic phase (*16*, *17*). Given the inherently low thermal conductivity of the polymer shell and the ultrathin shell thickness (1 to 2 nm), it is reasonable to assume that the inorganic core would dominate thermal transport. Together, these effects in a hybrid material could offer an unprecedented opportunity to decouple thermal and electrical transport to engineer a high ZT value. However, there has been no experimental demonstration of this approach, and the size (i.e., diameter) dependence of electronic and thermal transport for the hybrid nanowires also remains unexplored.

Over the past decade, Te-PEDOT:PSS hybrids have been fabricated as bulk films using various fabrication methods, and the high thermoelectric performance has been attributed to the following possible mechanisms: (i) energy filtering at the organic-inorganic interface due to work function offset between the two constituents; (ii) interfacial charge transfer induced doping/de-doping; and (iii) locally enhanced transport at the Te and PEDOT:PSS interface due to structural reordering effects, i.e., templating (*12*–*15*, *18*–*20*). However, owing to the multiphase nature of these materials, the validity and contribution of these different mechanisms remain an issue of debate. This is further complicated by the fact that all thermoelectric transport studies on the Te-PEDOT:PSS hybrid system

[1]Energy Storage and Distributed Resources Division, Lawrence Berkeley National Laboratory, Berkeley, CA 94720, USA. [2]The Molecular Foundry, Lawrence Berkeley National Laboratory, Berkeley, CA 94720, USA. [3]Applied Science and Technology Graduate Group, University of California, Berkeley, Berkeley, CA 94720, USA. [4]Department of Materials Science and Engineering, University of California, Berkeley, Berkeley, CA 94720, USA. [5]National Center for Electron Microscopy, The Molecular Foundry, Lawrence Berkeley National Laboratory, Berkeley, CA 94720, USA. [6]College of Engineering, University of California, Berkeley, Berkeley, CA 94720, USA. [7]Department of Mechanical Engineering, University of California, Berkeley, Berkeley, CA 94720, USA. *Corresponding author. Email: rsprasher@lbl.gov (R.S.P.); jjurban@lbl.gov (J.J.U.) †These authors contributed equally to this work.

thus far have centered on bulk films (nanowire meshes fabricated into thin films, each containing billions of nanowires) (*12*–*15*, *18*–*20*). In these films, the measured thermoelectric properties are averaged over wires of varying dimensions and orientations, and interfacial scattering between nanowires makes it challenging to elucidate the inherent charge transport mechanism.

In addition, thermal transport in these hybrid systems has not been studied, although these multiphase materials could exhibit interesting phonon scattering mechanisms. For instance, molecular dynamics (MD) simulations of Si/amorphous SiO_2 (a-SiO_2), another core/shell nanowire containing a hard-soft interface, have shown that the presence of a-SiO_2 on the Si nanowire surface strongly scatters phonons propagating into the amorphous shell, forming quasi-stationary modes with mean free paths (MFPs) on the order of interatomic distances (*21*). In a similar manner, the semicrystalline PEDOT:PSS shell of the hybrid system is also acoustically soft and slow (*22*), in which case phonons are likely to form nonpropagating modes within it, thereby forcing thermal transport within the inorganic Te core, and a size (i.e., diameter)–dependent thermal conductivity is expected due to stronger phonon-boundary scattering. Furthermore, thermal conductivity measurements for hybrid thin films reported thus far have been measured in the through-plane direction, while charge transport and electronic properties are measured in the in-plane direction (*3*). This has led to inconsistencies in the literature, especially given the inherently anisotropic nature of a bulk mesh film. Hence, to glean insight into the underlying charge carrier and phonon transport mechanisms, a model material system comprising free-standing single hybrid nanowires is required with electronic and thermal properties measured along the same axial direction. Performing a systematic and well-controlled study on such a model system will enable the establishment of structure-property relationships for hybrid materials, which is of paramount importance to enhance thermoelectric performance.

In this work, we report the thermoelectric properties of individual free-standing Te-PEDOT:PSS core/shell nanowires. By varying the diameter of the inorganic core while maintaining a fixed organic shell thickness, we directly demonstrate that the PEDOT:PSS shell dominates charge carrier (hole) transport. An inverse relationship between the electrical and thermal conductivity with respect to nanowire diameter confirms the ability to decouple these properties, with the inorganic core being the dominant channel for phonon transport. Our results demonstrate the unique advantage of using hybrid materials for thermoelectric applications and provide critical insight into the mechanisms at play, as described in the following sections.

RESULTS

Thermoelectric properties of single hybrid nanowires

The nanowires used in this study consist of a soft polymer shell (PEDOT:PSS) and a hard inorganic core (Te) that appears to be single crystal belonging to space group $P3_121$ as shown in Fig. 1 (A and C). The thermoelectric properties of individual Te-PEDOT:PSS nanowires were measured using a custom-fabricated suspended microheater device shown in Fig. 1B (*23*–*25*), which enables simultaneous measurement of σ, *S*, and κ on the same nanowire sample (see Materials and Methods) (*26*, *27*). This sample geometry ensures that both

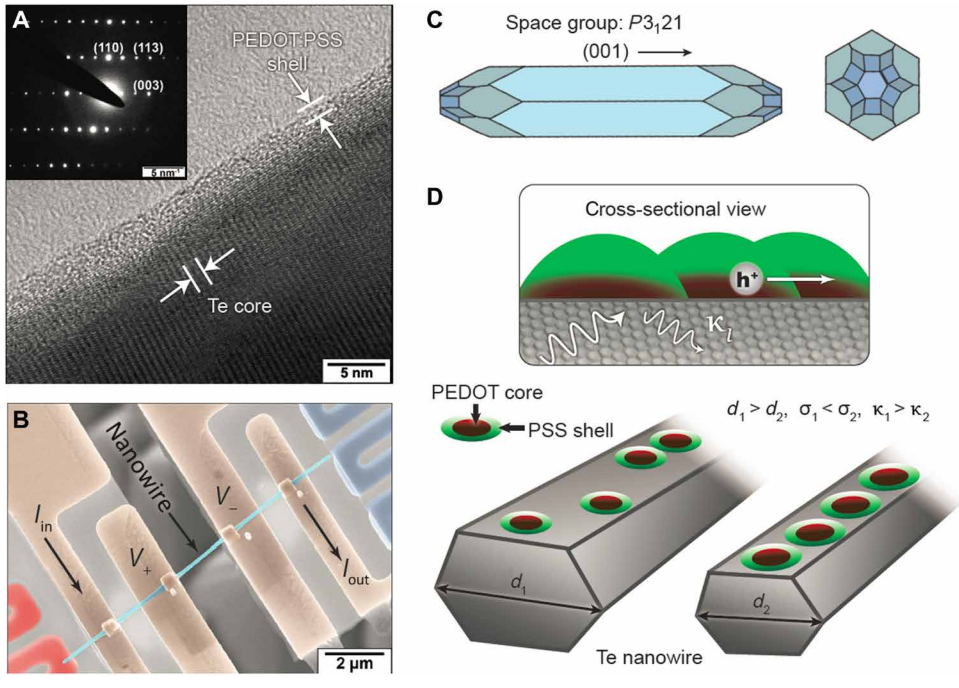

Fig. 1. Material structure and thermoelectric property measurement scheme. (**A**) A high-resolution transmission electron microscope micrograph distinguishing between the PEDOT:PSS shell and the inorganic Te core. The inset is an SAED pattern confirming the single-crystal nature of the Te nanowire and its crystallographic structure and orientation. (**B**) Scanning electron micrograph depicting the suspended pad measurement platform used to probe the thermoelectric properties of the hybrid nanowire, where the artificial coloration is used to aid in distinguishing between components. (**C**) Visualization of the crystallographic space group that the Te core forms with the different facets shown and the (001) direction along the nanowire axis of growth. (**D**) The top portion of the cartoon schematics depicts thermal transport occurring through the inorganic core while electronic carrier transport is occurring through the organic shell, and the bottom portion of the panel illustrates the proposed hypothesis of better organic templating on narrower nanowire diameters being the cause for the observed enhanced charge mobility.

thermal and electrical properties are measured along the same axial direction, which is crucial given the anisotropic nature of these hybrids, and addresses a major drawback with previous thin film measurements.

The room temperature electronic properties of Te-PEDOT:PSS core/shell nanowires with six different diameters are shown in Fig. 2. The smallest sample measured has a diameter of ~40 nm due to challenges associated with dry transferring thinner nanowires. The value of σ monotonically increases from 10.8 to 43.1 S/cm as the nanowire diameter (D) is reduced from 186 to 42 nm, while S remains nearly constant at ~302 μV/K across all samples, collectively resulting in a power factor increase from 90 to 415 μW/m-K^2. Here, the electrical conductivity is calculated on the basis of $\sigma = L/(RA)$, where L is the nanowire suspended length, R is the measured electrical resistance, and A is the total cross-sectional area of the hybrid nanowire. Thus, by reducing the wire diameter in this hybrid system, we are able to achieve a monotonic increase in σ, while S remains largely unchanged. This trend contrasts with single-phase materials, in which a fundamental inverse relationship between S and σ upon doping limits enhancements to the power factor. Note that for all core/shell nanowires studied in this work, the PEDOT:PSS polymer shell thickness is 1.45 ± 0.34 nm, while the Te core diameter is varied (fig. S1), and the suspended length of all wires is maintained between 2.8 and 3.7 μm.

To understand the underlying mechanisms for the diameter dependence of σ that results in a power factor enhancement, it is critical to consider what material phase (i.e., inorganic or organic) dominates electrical transport in the hybrid. If the inorganic core dominates transport, reducing the diameter would not affect σ for wires with diameters larger than the electron MFP; when the diameter is smaller than the electron MFP, σ would be lower due to electron-boundary scattering effects, unless the material is a topological insulator (*28*). However, theoretical predictions show that Te becomes a topological insulator only with the application of shear strain (*29*), which is absent in our experiments. A second possible mechanism is energy filtering at the hard-soft interface due to the work function

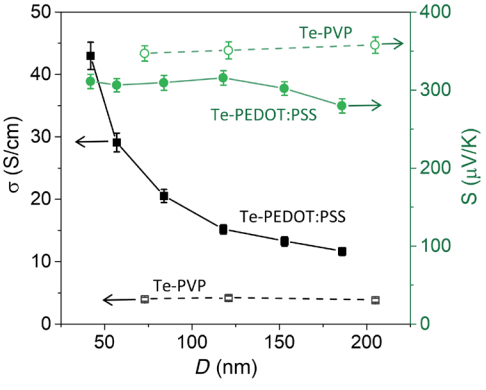

Fig. 2. Room temperature electrical transport properties. Measured room temperature electrical conductivity and Seebeck coefficient are plotted as a function of wire diameter for different Te-PEDOT:PSS core/shell nanowires. The measured results of Te-PVP core/shell nanowires, represented by the hollow symbols, are also plotted for comparison. Note that PVP is an electrical insulator, and similar to the Te-PEDOT:PSS wires, the PVP layer thickness is kept at ~1.14 ± 0.36 nm in Te-PVP nanowires, while only the Te core diameter is varied. Here, the measurement uncertainties of σ are mainly from the uncertainties in nanowire length and diameter measurements, and uncertainties of S are mainly from the uncertainties in linear least square fitting.

offset between Te and PEDOT:PSS, which would cause the scattering of low-energy carriers and results in enhancements in S with only a modest decrease in σ (*18*). Given that all the nanowires studied here are composed of the same hard and soft material (i.e., same work function offset across the different samples), they would all be subject to the same energy-filtering effect, if at all. Thus, the phenomenon of energy filtering is irrelevant to our study. However, another possibility for the diameter dependence is that as the nanowire diameter decreases, the volume fraction of PEDOT:PSS in the hybrid increases, which, in turn, leads to a higher σ. However, our mean field theory calculation using the parallel resistance model rules out this effect, and the observed thermoelectric property enhancement cannot be described by a simple composite (details can be found in section S5). Thus, we hypothesize that electronic transport is occurring predominantly through the organic shell of the hybrid nanowire system.

To validate this hypothesis, we measured the thermoelectric properties of another set of nanowires with a different organic component, namely, polyvinylpyrrolidone (PVP)–coated Te nanowires. Unlike PEDOT, PVP is an electrical insulator but has a similar shell thickness of ~1.14 ± 0.36 nm, while the Te core diameter is varied (fig. S1). As shown in Fig. 2, the measured σ of Te-PVP core/shell nanowires is only 3.8 S/cm, and it does not exhibit a diameter dependence. If the Te core is responsible for charge transport in the hybrid system, Te-PVP would also show a size-dependent σ similar to Te-PEDOT:PSS wires. Note that transport through the organic shell has been previously proposed by Coates *et al.* (*13*) and Kumar *et al.* (*17*) based on bulk films, but our work provides experimental evidence that conclusively proves that charge transport occurs predominantly through the PEDOT:PSS shell.

With electronic transport occurring predominantly through the organic component, there are two possible mechanisms to explain the diameter dependence in these hybrids: interfacial charge transfer (doping/de-doping) and physical templating (structural reordering) at the interface. Interfacial charge transfer, also known as the de-doping effect, occurs at the organic-inorganic interface and results in an increase in the Seebeck coefficient of hybrid thin films compared to neat PEDOT:PSS films (*3*, *17*). In this case, the discrete molecular orbitals of the organic phase directly interact with continuum band states of the inorganic phase, resulting in interphase hole transfer from the organic PEDOT chain to the inorganic surface (*17*). This mechanism, in turn, would lead to an enhancement in S and a decrease in σ, which is inconsistent with our experimental results and thus fails to effectively capture the impact of nanowire diameter.

The other mechanism is physical templating of the organic phase on the inorganic surface. Due to the interaction between the organic shell and inorganic nanowire, theoretical work has shown that the packing of the PEDOT molecule is altered, resulting in a reorganization of polymer chains on the inorganic core that leads to larger crystalline PEDOT domains (*17*). It is well established that such changes in crystallinity and structural ordering of polymeric domains are correlated to carrier mobility, thus contributing to a larger electrical conductivity in PEDOT:PSS (*1*). Hence, we posit that this templating effect at the organic-inorganic interface is responsible for the observed performance enhancement and diameter dependence in Te-PEDOT:PSS single nanowires.

Charge transport in hybrid nanowires

Given that charge transport is dominated by the organic shell, we use the Kang-Snyder charge transport model to validate our hypothesis

that templating at the hard-soft interface leads to electrical conductivity enhancements with shrinking nanowire diameter, by separating contributions to transport that arise from mobility improvement and energy alignment (*30*). This model was initially developed for conducting polymers, and in contrast to various hopping or mobility edge models that are restricted to certain property regimes, the generalized Kang-Snyder model describes both the temperature and energy dependence of many polymers over eight orders of magnitude in electrical conductivity (*30*). The electrical conductivity σ can be characterized by the transport function $\sigma_E(E,T)$ as

$$\sigma = \int \sigma_E(E,T)\left(-\frac{\partial f}{\partial E}\right)dE \quad (1)$$

where f is Fermi-Dirac distribution function, and $\sigma_E(E,T)$ is the energy-dependent conductivity. The Seebeck coefficient can be described by the transport function $\sigma_E(E,T)$

$$S = \frac{1}{\sigma}\left(\frac{k_B}{e}\right)\int\left(\frac{E-E_F}{k_B T}\right)\sigma_E(E,T)\left(-\frac{\partial f}{\partial E}\right)dE \quad (2)$$

where E_F is Fermi level, and k_B is Boltzmann constant (more details in Materials and Methods). This model independently treats energy-dependent scattering (s), doping (reduced chemical potential η), and energy-independent transport [$\sigma_{E0}(T)$, which represents an effective carrier mobility].

A critical aspect in this model is the energy-dependent scattering parameter s, which distinguishes most conducting polymers ($s = 3$) from PEDOT-based polymers ($s = 1$) (*17*, *30*). Different s values are attributed to different charge transport mechanisms, and it has been shown that materials with $s = 1$ (analogous to acoustic phonon scattering in inorganic materials) generally exhibit a higher mobility than those with $s = 3$ (analogous to ionized impurity scattering in inorganic materials) (*30*, *31*). The applicability of this model to hybrid systems was previously demonstrated in hybrid thin films of Te(Cu_x)-PEDOT:PSS (*17*). In that work, Kumar *et al.* (*17*) assumed $s = 1$ and showed a good fit to their measured σ-S curve at varying amounts of Cu loading. Rather than assuming that $s = 1$ is the appropriate transport parameter for hybrid systems, our single-nanowire model system provides direct experimental validation for this—by comparing Te-PEDOT:PSS with Te-PVP wires (Fig. 2), we confirm that the PEDOT:PSS shell dominates charge transport and validate the use of the $s = 1$ parameter to model transport in hybrid Te-PEDOT:PSS nanowires.

For a given scattering parameter s, the reduced chemical potential $\eta(T)$ is obtained from the measured Seebeck coefficient $S(T)$, and then the transport coefficient $\sigma_{E0}(T)$ is extracted from the measured electrical conductivity $\sigma(T)$ (see Materials and Methods). The temperature-dependent S and σ values of these single nanowires, measured using the same suspended microheater experimental setup described earlier, are shown as in Fig. 3 (A and B, respectively).

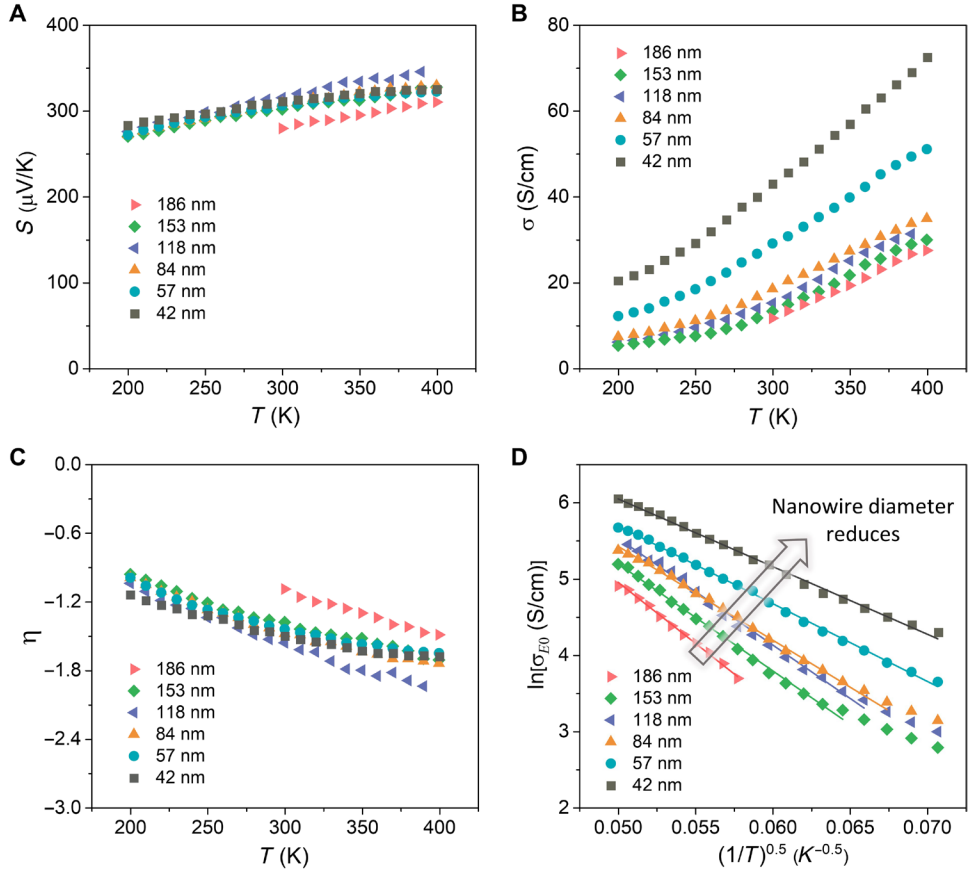

Fig. 3. Kang-Snyder model on temperature-dependent electrical transport properties. (**A** and **B**) Measured temperature-dependent Seebeck coefficient and electrical conductivity of Te-PEDOT:PSS hybrid nanowires with different diameters. (**C**) Reduced chemical potential $\eta = (E_F - E_t)/k_BT$ of different-diameter Te-PEDOT:PSS nanowires plotted as a function of temperature. (**D**) $\ln(\sigma_{E0})$ is plotted as a function of $T^{-0.5}$, and hopping energy W_γ is extracted by taking the slope of $\ln(\sigma_{E0})$ versus $T^{-0.5}$ curve.

The extracted $\eta(T)$ and $\sigma_{E0}(T)$ for wires with different diameters are shown in Fig. 3 (C and D), and Table 1 shows the room temperature results. It can be seen that σ_{E0}, which functions as an effective mobility and provides insight on the morphology of the polymer shell, increases monotonically as the wire diameter is reduced, reaching 213.5 S/cm for the 42-nm-diameter nanowire. The increasing trend of σ_{E0} suggests enhanced ordering of PEDOT moieties on the inorganic surfaces as the wire diameter reduces. On the other hand, η decreases slightly from −1.09 to −1.56 as the diameter is reduced from 186 to 118 nm and nearly saturates with further reduction in diameter. The change in $\eta(T)$ is much smaller than that in $\sigma_{E0}(T)$, suggesting that de-doping effects that are captured in the reduced chemical potential are not important in explaining the diameter dependence of these hybrid nanowires. This is as expected since de-doping at the interface results in trends that are opposite to what we measure experimentally for these hybrid nanowires. To further investigate the role of morphology in the observed performance enhancements, we calculate the hopping energy W_γ, which represents the energy barrier for transport between ordered regions, from $\sigma_{E0}(T)$

$$\sigma_{E0} \sim \exp\left[-\left(\frac{W_\gamma}{k_B T}\right)^\gamma\right] \quad (3)$$

Here, $\gamma = {}^1/_2$ is chosen as it is widely used for polymers, including PEDOT:PSS (*30*). As shown in Table 1, W_γ decreases from 2.13 to 0.68 eV as the wire diameter is reduced from 186 to 42 nm. A lower W_γ value is expected for polymer films with improved long-range morphological order (*30*), and this confirms that nanowire diameter reduction results in an enhancement in the templating effect of the organic shell on the inorganic core that increases charge carrier mobility, thus leading to a boost in electrical conductivity.

Although the impact of morphology on σ or W_γ is relatively straightforward to understand, its impact on S or η is less clear. It has been shown that higher degrees of PEDOT crystallinity can increase the number of available states around the Fermi level (*32*), which would result in an increase in the Seebeck coefficient. However, as shown by Patel *et al.* (*33*), the Seebeck coefficient is less sensitive to morphological order as compared to electrical conductivity, and this could possibly explain the roughly constant value in the measured S [and is reflected in the small change of $\eta(T)$ in Table 1]. Notably, we posit that the high Seebeck coefficient of the PEDOT shell is due to interphase hole transfer from the organic PEDOT chain to the inorganic Te surface, i.e., de-doping effects occurring at the interface, as predicted by previous theoretical simulations (*17*). This interfacial charge transfer or de-doping leads to a lower charge carrier concentration of the PEDOT phase and results in a high Seebeck coefficient. Similar Seebeck coefficients have also been experimentally measured in PEDOT by reducing the charge carrier concentration (*34*–*36*). As has been shown in organic materials, Seebeck coefficient is dominated by carrier concentration (i.e., de-doping effects at the hard-soft interface) and is much less sensitive to charge carrier mobility (i.e., morphological effects such as templating) (*33*). Since the increase in electrical conductivity with reduced nanowire diameter is caused by mobility enhancements, it is expected that the Seebeck coefficient remains relatively unchanged for nanowires of varying diameter measured in this work.

Table 1. Electrical transport parameters extracted using the Kang-Snyder model based on the measured room temperature results for Te-PEDOT:PSS core/shell nanowires with different diameters.

Diameter (nm)	Reduced chemical potential, η	Transport coefficient, σ_{E0} (S/cm)	Hopping energy, W_γ (eV)
186	−1.09	40.12	2.13
153	−1.38	59.01	1.69
118	−1.56	79.45	1.59
84	−1.48	90.07	1.30
57	−1.44	136.78	0.90
42	−1.50	213.49	0.68

Gate-modulated electrical conductivity measurements

To quantify the mobility enhancement due to templating, which enhances the electrical conductivity of smaller-diameter Te-PEDOT:PSS core/shell nanowires, field effect–modulated experiments were conducted (details in section S6), as has been previously reported for Sb_2Te_3 nanowires (*37*) and Ge-Si core/shell nanowires (*38*). Three nanowires with different diameters were measured, and the formation of ohmic contact between the nanowire and the metal electrodes was confirmed by the linear current-voltage relation (I-V) curves at various gate voltages (fig. S10A). As confirmed earlier, since the electrical current primarily flows through the organic shell in Te-PEDOT:PSS nanowires, the measured source-drain current I_{DS} can be approximated as $I_{DS} = \frac{V_{DS}}{R_{shell}} = \frac{V_{DS}\sigma_{shell}\pi Dt}{L}$, where V_{DS} is the source-drain voltage, σ_{shell} is the polymer shell electrical conductivity, D is the nanowire diameter, t is the shell thickness, and L is the nanowire length. In contrast to conventional single-phase nanowires in which the measured I_{DS} is normalized by the cross-sectional area, as shown in Fig. 4A, the shell cross-sectional area over length normalization [$I_{DS}^* = I_{DS}/(\pi Dt/L)$] is used to ensure a meaningful comparison between different diameter hybrid nanowires, where V_{DS} is kept at 0.2 V. As expected, all nanowires show increased I_{DS}^* as V_G reduces, as a result of p-type behavior and hole transport. I_{DS}^* increases for nanowires with smaller diameter at $V_G = 0$, which provides evidence that σ_{shell} increases as the core diameter reduces.

The enhancement in the shell electrical conductivity can be related to hole mobility, which is extracted using the calculated transconductance g_m from the measured I_{DS}-V_G data (fig. S10B) as $\mu = (g_m L^2)/(V_{DS}C)$, where C is the capacitance of the gate oxide (details can be found in section S6) (*38*). Figure 4B shows the hole mobility, which increases from 9.46 to 20.5 cm^2/Vs as the wire diameter reduces from 191 to 67 nm; this mobility value is very close to that of PEDOT thin films (26.6 cm^2/Vs) synthesized using oxidative chemical vapor deposition (*39*), thus confirming the high crystallinity and morphological order of the organic shell in the hybrid. Moreover, the mobility increase follows the same increasing trend as the Kang-Snyder model transport coefficient σ_{E0} with reducing wire diameter. Thus, both approaches (qualitative and quantitative) independently validate the hypothesis that increased carrier mobility due to morphological ordering (templating) is responsible for the enhanced thermoelectric performance in smaller-diameter wires.

To understand the driving force and extent of templating in different nanowires, we must consider how PEDOT chains interact with the Te nanowire surface as diameter reduces. The morphology

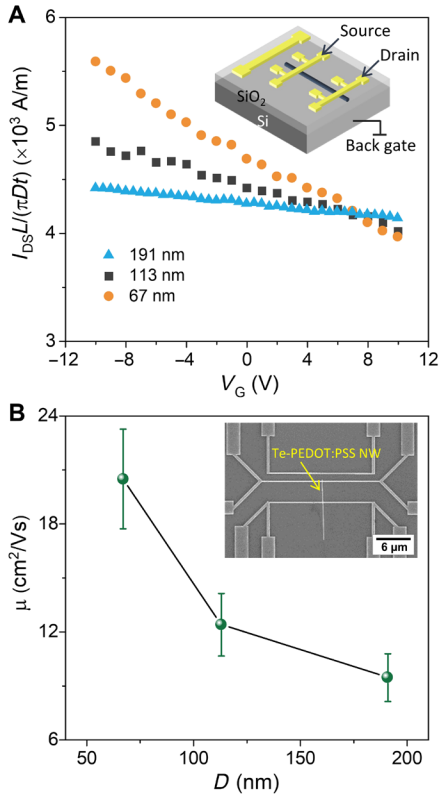

Fig. 4. Gate-modulated electrical conductivity measurements. (**A**) Measured source-drain current normalized with respect to the ratio of nanowire (NW) shell cross-sectional area over length [$I_{DS}^* = I_{DS}/(\pi Dt/L)$] of three Te-PEDOT:PSS core/shell nanowires as a function of gate voltage, V_G, where the source-drain voltage, V_{SD}, is kept at 0.2 V. Inset: Schematic drawing of the device. (**B**) Hole mobility, μ, plotted as a function of nanowire diameter, *D*. Inset: Scanning electron microscope image of the device used for the gated electrical conductivity measurements. The measurement uncertainties of μ are mainly from the uncertainties in nanowire length and diameter measurements.

of polymeric materials is typically characterized via a variety of techniques such as grazing incidence wide/small-angle x-ray scattering, atomic force microscopy, and electron diffraction (*40*–*42*). While the structure of PEDOT:PSS has been effectively resolved through these methods, the polymer blend itself is typically semi-amorphous, resulting in a lack of strong scattering peaks that are common in other conjugated polymers (*43*, *44*). This fact, paired with the ultrathin nature of the organic shell (1 to 2 nm thick) seated on top of a highly ordered, inorganic Te core, makes it exceedingly difficult to experimentally obtain the structural detail of the polymer shell in the hybrid. Nevertheless, we can leverage recent theoretical work to provide some insight on the improved structural order of the polymer chains as the Te core diameter reduces (*17*, *45*–*47*). As demonstrated by Ouyang *et al.* (*45*) and Ghosh *et al.* (*46*), surface energy of Te nanowires is directly proportional to the nanowire diameter. Thus, as the diameter decreases, this suppression of surface energy would facilitate polymer self-assembly on the nanowire surface (*17*, *47*). Furthermore, MD simulations performed by Kumar *et al.* (*17*) reveal that a ~2× reduction in interaction energy at the interface of Te-PEDOT as compared to $Cu_{1.75}$Te-PEDOT facilitates the movement of PEDOT chains, thus enabling improved self-assembly. The question of epitaxial polymer crystallization is a complex one that is dependent on various factors, such as temperature, polymer-inorganic facet interaction energy, and polymer chain mobility (*48*). On the basis of the results of this study, we posit that as the wire diameter shrinks, the polymer shell crystallites become more ordered, greatly enhancing the local and long-range connectivity of the organic shell, as shown in Fig. 1D. We expect this effect to plateau as the inorganic core diameter approaches the polymer crystallite size, which acts as the inherent ordering limit (near single crystal). Theoretical calculations have shown that a maximum power factor of ~31,200 μW/m-K^2 could be achieved at a carrier concentration of 6.5×10^{19} cm^{-3} for single-crystal PEDOT (*49*), which is the upper limit for the thermoelectric power factor of the ordered polymer shell in this hybrid nanowire. However, future experiments and theoretical modeling are needed to provide further insight on the exact mechanism for the high thermoelectric power factor in this hybrid material system.

Thermal transport in hybrid nanowires

With the organic shell confirmed to be the primary channel for charge transport, the next step is to reveal the role of organic shell and inorganic core in thermal transport. To this end, we performed temperature-dependent thermal conductivity measurements on the same set of individual Te-PEDOT:PSS hybrid nanowires of different diameters. As shown in Fig. 5A, the measured κ value of the largest nanowire is 2.01 W/m-K at 300 K, and it shows a continually decreasing trend as the diameter reduces, reaching 0.68 W/m-K for the 42-nm-diameter nanowire. Combined with the measured power factor, these collectively result in a ~14× enhancement in *ZT* compared to the 186-nm-diameter nanowire, reaching a value of 0.18 at 300 K (Fig. 5B), and an even higher *ZT* value of 0.54 is achieved at 400 K (Fig. 5C). Traditional efforts to suppress thermal transport in thermoelectric materials typically result in an adverse impact on σ due to increased scattering events or a decrease in carrier concentration (*8*). Our results reveal that by reducing the wire diameter, we are able to reduce κ while simultaneously increasing σ to obtain an enhanced thermoelectric *ZT* in Te-PEDOT:PSS nanowires (Fig. 5D). Note that the *ZT* value achieved (0.54 at 400 K) for these undoped individual nanowires is the highest among all Te-PEDOT:PSS materials prepared under various conditions (*12*–*15*, *18*–*20*), and our measurement technique ensures the highest accuracy as all three parameters (σ, *S*, and κ) are measured along the same axial direction of the same sample, unlike in previous thin-film measurements.

To quantify the electronic contribution to thermal transport, we estimate the electronic thermal conductivity based on the Wiedemann-Franz law as $\kappa_e = L\sigma T$, where *L* is the Lorenz number. For the 42-nm-diameter wire, the estimated κ_e value based on the degenerate limit is 0.03 W/m-K at 300 K, which highlights the negligible role of electrons in thermal transport in this system. This is further confirmed by performing temperature-dependent κ measurements that follow approximately a $1/T$ relation above 300 K (Fig. 5A), signifying the dominant role of Umklapp phonon scattering. In addition, phonons as the dominant heat carriers in these hybrids are confirmed by measurements on Te-PVP nanowires that show thermal conductivity values that are similar to Te-PEDOT:PSS nanowires of comparable diameters (Fig. 5A). If electrons were contributing substantially to thermal transport, a much lower κ value should be observed for Te-PVP wires based on the fact that their σ value is at least 3× lower than that of Te-PEDOT:PSS (Fig. 2). This establishes phonons as the dominant heat carriers in this system, and it is now

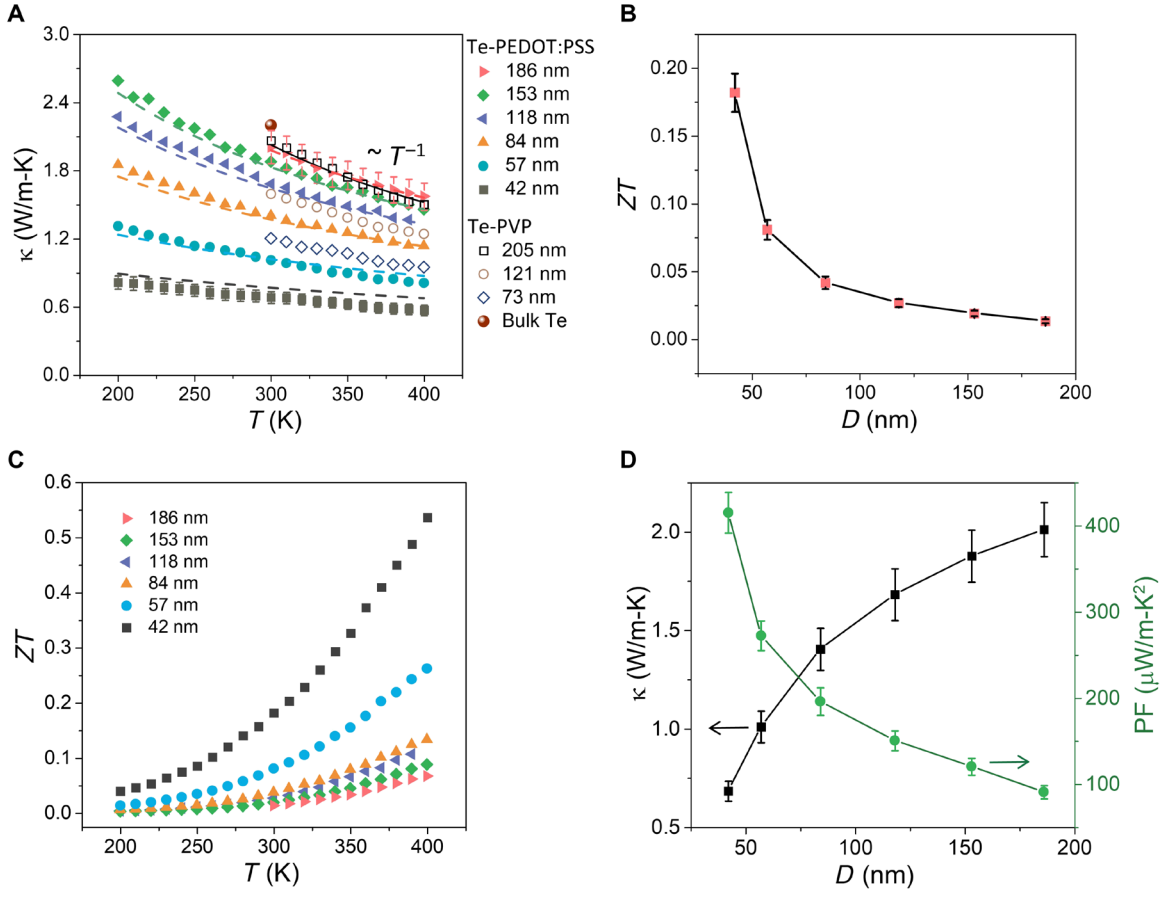

Fig. 5. Thermoelectric properties of hybrid nanowires. (**A**) Temperature-dependent thermal conductivity of Te-PEDOT:PSS and Te-PVP nanowires with different diameters, where the measured room temperature thermal conductivity for bulk Te is also plotted for comparison (*55*). The dashed lines are modeled thermal conductivity of each nanowires considering the effects of phonon-boundary scattering. (**B**) Size-dependent thermoelectric figure of merit, *ZT*, of Te-PEDOT:PSS hybrid nanowires at room temperature. (**C**) Temperature-dependent *ZT* of Te-PEDOT:PSS hybrid nanowires with various diameters. (**D**) Size-dependent thermal conductivity and power factor of Te-PEDOT:PSS hybrid nanowires at room temperature, which show inverse relationship with respect to the nanowire diameter. Here, the measurement uncertainties of κ are mainly from the uncertainties in nanowire length and diameter measurements, and the uncertainties of *ZT* are calculated on the basis of the respective uncertainties in *S*, σ, and κ.

possible to understand the size dependence of κ. MD simulations on other hybrids such as Si/a-SiO_2 core/shell nanowires have shown that quasi-stationary modes that formed in the amorphous shell carry heat much less efficiently than the propagating phonon modes in the crystalline core (*21*). On the basis of the measured κ value of semicrystalline PEDOT:PSS (0.5 W/m-K) (*50*) and shell thickness of ~1.45 nm, we calculate that the organic shell contributes less than 13% to the total thermal transport using the simple parallel resistance model (details in section S8). In addition, prior theoretical work has shown that 90% of thermal transport along the axial direction in Te can be attributed to phonons with an MFP less than 200 nm (*51*). Thus, as the nanowire diameter reduces, phonon-boundary scattering becomes increasingly important and will act to suppress the overall thermal conductivity. This effect can be clearly seen from the flattened κ(*T*) curves for nanowires with shrinking diameter (Fig. 5A). As a result, we posit that the inorganic core is the dominant channel for thermal transport, and the overall reduction in κ value for smaller-diameter nanowires is due to the increased impact of phonon-boundary scattering.

To confirm this hypothesis, we modeled the lattice thermal conductivity of the hybrid nanowire based on the Callaway-Holland model (details in section S8) (*52*, *53*). In the calculation, we only consider thermal transport in the Te core and neglect the contribution of the thin PEDOT:PSS shell. The calculation is performed along the nanowire axial direction based on the phonon dispersion relation of bulk Te (*51*). We consider the mode-dependent phonon relaxation time using Matthiessen's rule, taking into account Umklapp, boundary, and defect scattering mechanisms (*52*, *53*). The dashed lines in Fig. 5A are modeled temperature-dependent κ values in which only the phonon-boundary scattering term is altered on the basis of nanowire diameter, showing excellent agreement with the experimental results.

DISCUSSION

Although Te-PEDOT:PSS is not a new hybrid material system and has been widely studied in previous work (*12*–*15*, *18*–*20*), by using a carefully controlled single-nanowire transport study, we have been able to experimentally capture the effects of nanoscale templating at the organic-inorganic interface, which helps to fill in the knowledge gap between atomic-scale simulations (*17*) and bulk thin-film measurements (*12*–*15*, *18*–*20*). Our findings reveal that in nanostructured

hybrid materials comprising a thin electrically conductive organic shell coated on a crystalline inorganic core, electrical transport predominantly occurs through the organic shell, while thermal transport is primarily driven by the inorganic core, thereby offering an avenue to decouple these notoriously linked parameters for thermoelectric applications. Because of the fundamental nature of this study, it should be noted that the materials discussed are undoped and have not undergone additional postprocessing. Thus, there is great potential to further optimize the thermoelectric properties and achieve even higher *ZT* values. Furthermore, the insight gained from this model system helps establish a framework for next-generation organic-inorganic hybrid thermoelectric materials through the design principles of interfacial energy minimization (for improved morphology and long-range order) and favorable energetic pairing for optimal de-doping effects (for improved electronic energetics) between the hard and soft components. From these insights, it is possible to envisage the rational design of a plethora of high-performing, advanced materials composed of new pairings of inorganic nanostructures (perhaps with more environmentally friendly options such as bismuth or sulfur) with conjugated polymers and small molecules to design new p-type materials and more elusive n-type hybrids as well.

In summary, through combining thermoelectric property measurements on single Te-PEDOT:PSS nanowires with the Kang-Snyder model and gate-modulated electrical conductivity experiments, we show that electrical conductivity is enhanced at smaller nanowire diameter due to an increase in the charge carrier mobility of the PEDOT:PSS shell, which, in turn, is attributed to a physical templating effect at the organic-inorganic interface. Simultaneously, thermal conductivity is reduced at smaller-diameter nanowires due to strong phonon-boundary scattering in the Te core. Specifically, for the hybrid nanowire with the smallest diameter of 42 nm, a σ value of 43.1 S/cm, *S* value of 310.9 μV/K, and a low κ value of 0.68 W/m-K are achieved, translating to a *ZT* value of 0.18 at 300 K. For this same nanowire, an even greater *ZT* value of 0.54 can be achieved at a temperature of 400 K, which is, to the best of our knowledge, the highest *ZT* value achieved to date for this hybrid material. These results demonstrate the ability to decouple electronic and thermal properties in organic-inorganic hybrid materials for thermoelectric applications. Our work provides valuable insights to guide the design of an ideal hybrid material with precise control over the interaction between the organic and inorganic phases for a vast array of different electronic materials and applications.

MATERIALS AND METHODS

Material synthesis

Synthesis of Te-PEDOT:PSS core/shell nanowires was performed according to the ligand exchange procedure published by Sahu *et al.* (*54*). PEDOT:PSS (Clevios PH1000) was purchased from Heraeus and was vortexed and filtered but otherwise underwent no further processing. Tellurium dioxide (99.9995%), PVP (average molecular weight, 40 kDa), sodium hydroxide (Sigma-Aldrich reagent, ≥97.0%, pellets), ethylene glycol (ReagentPlus, ≥99%), hydrazine hydrate (78 to 82%, iodometric), and sodium sulfide were purchased from Sigma-Aldrich. The single-crystal Te nanowires are initially synthesized with PVP as the surface ligand to act as the structure directing agent. Once synthesized, the wires then undergo a multistep ligand exchange procedure where the final product is coated with a thin conformal layer of PEDOT:PSS. Hybrid nanowires are then drop-casted onto glass substrates.

Structural characterization

An FEI Titan 60-300 microscope was operated at an accelerating voltage of 200 kV. Real-space images were taken with a spot size of 3 and an exposure of 0.5 s for all structures. Selected-area electron diffraction (SAED) was taken for three nanowires with slightly different conditions. For all structures, an SAED aperture of 40 μm and a camera length of 160 mm were used. For nanowires with diameters of 50 and 80 nm, a spot size of 7 and an exposure of 0.5 s were used. For the nanowire with a diameter of 170 nm that was imaged, a spot size of 9 and exposure of 0.3 s were used. For additional polymer shell thickness characterization, an FEI monochromated F20 UT Tecnai was operated at an accelerating voltage of 200 kV. Real-space images were taken with a spot size of 3 and an exposure of 0.7 s.

Thermoelectric property measurements on individual nanowires

For thermoelectric measurements, the hybrid nanowire meshes were first immersed in reagent alcohol and sonicated for ~10 s, and the nanowire suspension was then drop-casted on a piece of polydimethylsiloxane. Next, an individual nanowire was picked up by a sharp probe, mounted on an in-house assembled micromanipulator, and laid between two side-by-side suspended membranes integrated with microheaters/thermometers. The thermoelectric properties of individual nanowires were measured in a cryostat (Janis VPF-800) operated under a high vacuum ($<1 \times 10^{-6}$ mbar) with a dual radiation shield configuration. EBID (electron beam induced deposition) of the Pt/C composite was performed at the contacts between the nanowire and Pt electrodes using a dual-beam system (focused ion beam–scanning electron microscope, FEI Quanta) to establish good electrical contacts and minimize the contact thermal/electrical resistance. The electrical resistance measurement was performed before thermal measurements at each designated temperature point using the four-probe method. During the measurements, we used a DC voltage output from the data acquisition board (National Instruments PCI-6052e), which was connected to a large resistor (1 megohm) in series with the outer electrodes of the microdevice. By varying the output DC voltage, a sweeping DC current was applied to the Te-PEDOT:PSS nanowire, with the voltage difference between the two inner electrodes measured by a voltage amplifier (Stanford Research Systems, SR560), and the DC current was recorded by a high-accuracy current amplifier (Keithley 6487). The temperature-dependent electrical resistance [$R(T)$] of each measured sample is subsequently obtained by fitting the linear *I*-*V* curve.

To increase the sensitivity for thermal connectivity measurements, a Wheatstone bridge circuit was adopted through introducing a blank device, which helps to reduce the noise from the temperature fluctuations of the sample holder. During the thermal measurements, we also measured the Seebeck coefficient for each sample by monitoring the temperature difference of the two suspended membranes and the induced voltage difference (SR560) across the two inner electrodes.

Kang-Snyder charge transport model

The transport function $\sigma_E(E,T)$, also regarded as energy-dependent conductivity, can be described by

$$\sigma_E(E,T) = \sigma_{E0}(T)\left(\frac{E-E_t}{k_B T}\right)^s \quad (4)$$

Through integrating by parts, Eqs. 1 and 2 simplify to

$$\sigma = \sigma_{E0}(T) \times sF_{s-1}(\eta) \quad (5)$$

and

$$S = \frac{k_B}{e}\left[\frac{(s+1)F_s(\eta)}{sF_{s-1}(\eta)} - \eta\right] \quad (6)$$

respectively. Here, F is the complete Fermi-Dirac integral: $F_i(\eta) = \int_0^\infty \frac{\varepsilon^i}{1+e^{\varepsilon-\eta}} d\varepsilon$, and η is the reduced chemical potential: $\eta = (E_F - E_t)/k_B T$, where E_F is Fermi level, E_t is transport energy, below which there is no contribution to the conductivity, k_B is Boltzmann constant, and T is absolute temperature (*30*).

SUPPLEMENTARY MATERIALS

Supplementary material for this article is available at http://advances.sciencemag.org/cgi/content/full/7/20/eabe6000/DC1

REFERENCES AND NOTES

1. B. Russ, A. Glaudell, J. J. Urban, M. L. Chabinyc, R. A. Segalman, Organic thermoelectric materials for energy harvesting and temperature control. *Nat. Rev. Mater.* **1**, 16050 (2016).
2. J. J. Urban, A. K. Menon, Z. Tian, A. Jain, K. Hippalgaonkar, New horizons in thermoelectric materials: Correlated electrons, organic transport, machine learning, and more. *J. Appl. Phys.* **125**, 180902 (2019).
3. E. W. Zaia, M. P. Gordon, P. Yuan, J. J. Urban, Progress and perspective: Soft thermoelectric materials for wearable and Internet-of-Things applications. *Adv. Electron. Mater.* **5**, 1800823 (2019).
4. A. K. Menon, S. K. Yee, Design of a polymer thermoelectric generator using radial architecture. *J. Appl. Phys.* **119**, 055501 (2016).
5. M. A. Hannan, S. Mutashar, S. A. Samad, A. Hussain, Energy harvesting for the implantable biomedical devices: Issues and challenges. *Biomed. Eng. Online* **13**, 79 (2014).
6. H. M. Elmoughni, A. K. Menon, R. M. W. Wolfe, S. K. Yee, A textile-integrated polymer thermoelectric generator for body heat harvesting. *Adv. Mater. Technol.* **4**, 1800708 (2019).
7. M. Rein, V. D. Favrod, C. Hou, T. Khudiyev, A. Stolyarov, J. Cox, C. C. Chung, C. Chhav, M. Ellis, J. Joannopoulos, Y. Fink, Diode fibres for fabric-based optical communications. *Nature* **560**, 214–218 (2018).
8. R. Chen, J. Lee, W. Lee, D. Li, Thermoelectrics of nanowires. *Chem. Rev.* **119**, 9260–9302 (2019).
9. L. D. Hicks, M. S. Dresselhaus, Effect of quantum-well structures on the thermoelectric figure of merit. *Phys. Rev. B* **47**, 12727–12731 (1993).
10. A. I. Hochbaum, R. Chen, R. D. Delgado, W. Liang, E. C. Garnett, M. Najarian, A. Majumdar, P. Yang, Enhanced thermoelectric performance of rough silicon nanowires. *Nature* **451**, 163–167 (2008).
11. K. Biswas, J. He, I. D. Blum, C.-I. Wu, T. P. Hogan, D. N. Seidman, V. P. Dravid, M. G. Kanatzidis, High-performance bulk thermoelectrics with all-scale hierarchical architectures. *Nature* **489**, 414–418 (2012).
12. K. C. See, J. P. Feser, C. E. Chen, A. Majumdar, J. J. Urban, R. A. Segalman, Water-processable polymer-nanocrystal hybrids for thermoelectrics. *Nano Lett.* **10**, 4664–4667 (2010).
13. N. E. Coates, S. K. Yee, B. McCulloch, K. C. See, A. Majumdar, R. A. Segalman, J. J. Urban, Effect of interfacial properties on polymer-nanocrystal thermoelectric transport. *Adv. Mater.* **25**, 1629–1633 (2013).
14. S. K. Yee, N. E. Coates, A. Majumdar, J. J. Urban, R. A. Segalman, Thermoelectric power factor optimization in PEDOT:PSS tellurium nanowire hybrid composites. *Phys. Chem. Chem. Phys.* **15**, 4024–4032 (2013).
15. E. Jin Bae, Y. Hun Kang, K. S. Jang, S. Yun Cho, Enhancement of thermoelectric properties of PEDOT:PSS and tellurium-PEDOT:PSS hybrid composites by simple chemical treatment. *Sci. Rep.* **6**, 18805 (2016).
16. J. N. Heyman, B. A. Alebachew, Z. S. Kaminski, M. D. Nguyen, N. E. Coates, J. J. Urban, Terahertz and infrared transmission of an organic/inorganic hybrid thermoelectric material. *Appl. Phys. Lett.* **104**, 141912 (2014).
17. P. Kumar, E. W. Zaia, E. Yildirim, D. V. M. Repaka, S. W. Yang, J. J. Urban, K. Hippalgaonkar, Polymer morphology and interfacial charge transfer dominate over energy-dependent scattering in organic-inorganic thermoelectrics. *Nat. Commun.* **9**, 5347 (2018).
18. E. W. Zaia, A. Sahu, P. Zhou, M. P. Gordon, J. D. Forster, S. Aloni, Y. S. Liu, J. Guo, J. J. Urban, Carrier scattering at alloy nanointerfaces enhances power factor in PEDOT:PSS hybrid thermoelectrics. *Nano Lett.* **16**, 3352–3359 (2016).
19. H. Song, K. Cai, Preparation and properties of PEDOT:PSS/Te nanorod composite films for flexible thermoelectric power generator. *Energy* **125**, 519–525 (2017).
20. M. Culebras, A. M. Igual-Muñoz, C. Rodríguez-Fernández, M. I. Gómez-Gómez, C. Gómez, A. Cantarero, Manufacturing Te/PEDOT films for thermoelectric applications. *ACS Appl. Mater. Interfaces* **9**, 20826–20832 (2017).
21. Y. He, G. Galli, Microscopic origin of the reduced thermal conductivity of silicon nanowires. *Phys. Rev. Lett.* **108**, 215901 (2012).
22. A. Henry, Thermal transport in polymers 1. Introduction to polymers. *Annu. Rev. Heat Transf.* **17**, 485–520 (2013).
23. L. Shi, D. Li, C. Yu, W. Jang, D. Kim, Z. Yao, P. Kim, A. Majumdar, Measuring thermal and thermoelectric properties of one-dimensional nanostructures using a microfabricated device. *J. Heat Transf.* **125**, 881–888 (2003).
24. L. Yang, Y. Yang, Q. Zhang, Y. Zhang, Y. Jiang, Z. Guan, M. Gerboth, J. Yang, Y. Chen, D. Greg Walker, T. T. Xu, D. Li, Thermal conductivity of individual silicon nanoribbons. *Nanoscale* **8**, 17895–17901 (2016).
25. A. Mavrokefalos, M. T. Pettes, F. Zhou, L. Shi, Four-probe measurements of the in-plane thermoelectric properties of nanofilms. *Rev. Sci. Instrum.* **78**, 034901 (2007).
26. L. Yang, Y. Tao, J. Liu, C. Liu, Q. Zhang, M. Akter, Y. Zhao, T. T. Xu, Y. Xu, Z. Mao, Y. Chen, D. Li, Distinct signatures of electron–phonon coupling observed in the lattice thermal conductivity of $NbSe_3$ nanowires. *Nano Lett.* **19**, 415–421 (2019).
27. L. Yang, Q. Zhang, Z. Cui, M. Gerboth, Y. Zhao, T. T. Xu, D. G. Walker, D. Li, Ballistic phonon penetration depth in amorphous silicon dioxide. *Nano Lett.* **17**, 7218–7225 (2017).
28. Z. Luo, J. Tian, M. Srinivasan, Y. P. Chen, X. Xu, Large enhancement of thermal conductivity and Lorenz number in topological insulator thin films. *ACS Nano* **12**, 1120–1127 (2018).
29. L. A. Agapito, N. Kioussis, W. A. Goddard, N. P. Ong, Novel family of chiral-based topological insulators: Elemental tellurium under strain. *Phys. Rev. Lett.* **110**, 176401 (2013).
30. S. Dongmin Kang, G. Jeffrey Snyder, Charge-transport model for conducting polymers. *Nat. Mater.* **16**, 252–257 (2017).
31. V. I. Fistul', *Heavily Doped Semiconductors* (Springer New York, 1995).
32. C. Liu, J. Xu, B. Lu, R. Yue, F. Kong, Simultaneous increases in electrical conductivity and Seebeck coefficient of PEDOT:PSS films by adding ionic liquids into a polymer solution. *J. Electron. Mater.* **41**, 639–645 (2012).
33. S. N. Patel, A. M. Glaudell, K. A. Peterson, E. M. Thomas, K. A. O'Hara, E. Lim, M. L. Chabinyc, Morphology controls the thermoelectric power factor of a doped semiconducting polymer. *Sci. Adv.* **3**, e1700434 (2017).
34. O. Bubnova, Z. U. Khan, A. Malti, S. Braun, M. Fahlman, M. Berggren, X. Crispin, Optimization of the thermoelectric figure of merit in the conducting polymer poly(3,4-ethylenedioxythiophene). *Nat. Mater.* **10**, 429–433 (2011).
35. O. Bubnova, M. Berggren, X. Crispin, Tuning the thermoelectric properties of conducting polymers in an electrochemical transistor. *J. Am. Chem. Soc.* **134**, 16456–16459 (2012).
36. T. Park, C. Park, B. Kim, H. Shin, E. Kim, Flexible PEDOT electrodes with large thermoelectric power factors to generate electricity by the touch of fingertips. *Energy Environ. Sci.* **6**, 788–792 (2013).
37. Y. M. Zuev, J. S. Lee, C. Galloy, H. Park, P. Kim, Diameter dependence of the transport properties of antimony telluride nanowires. *Nano Lett.* **10**, 3037–3040 (2010).
38. J. Moon, J.-H. Kim, Z. C. Y. Chen, J. Xiang, R. Chen, Gate-modulated thermoelectric power factor of hole gas in Ge–Si core–shell nanowires. *Nano Lett.* **13**, 1196–1202 (2013).
39. X. Wang, X. Zhang, L. Sun, D. Lee, S. Lee, M. Wang, J. Zhao, Y. Shao-Horn, M. Dincă, T. Palacios, K. K. Gleason, High electrical conductivity and carrier mobility in oCVD PEDOT thin films by engineered crystallization and acid treatment. *Sci. Adv.* **4**, eaat5780 (2018).
40. A. Hexemer, P. Müller-Buschbaum, Advanced grazing-incidence techniques for modern soft-matter materials analysis. *IUCrJ.* **2**, 106–125 (2015).
41. J. K. Hobbs, O. E. Farrance, L. Kailas, How atomic force microscopy has contributed to our understanding of polymer crystallization. *Polymer* **50**, 4281–4292 (2009).
42. M. Brinkmann, Insights into the structural complexity of semi-crystalline polymer semiconductors: Electron diffraction contributions. *Mater. Chem. Front.* **4**, 1916–1929 (2020).
43. U. Lang, E. Müller, N. Naujoks, J. Dual, Microscopical investigations of PEDOT:PSS thin films. *Adv. Funct. Mater.* **19**, 1215–1220 (2009).
44. Q. Wei, M. Mukaida, Y. Naitoh, T. Ishida, Morphological change and mobility enhancement in PEDOT:PSS by adding co-solvents. *Adv. Mater.* **25**, 2831–2836 (2013).
45. G. Ouyang, X. L. Li, X. Tan, G. W. Yang, Surface energy of nanowires. *Nanotechnology* **19**, 045709 (2008).
46. P. Ghosh, M. U. Kahaly, U. V. Waghmare, Atomic and electronic structures, elastic properties, and optical conductivity of bulk Te and Te nanowires: A first-principles study. *Phys. Rev. B - Condens. Matter Mater. Phys.* **75**, 245437 (2007).

47. F. Zhang, E. Mohammadi, X. Luo, J. Strzalka, J. Mei, Y. Diao, Critical role of surface energy in guiding crystallization of solution-coated conjugated polymer thin films. *Langmuir* **34**, 1109–1122 (2018).
48. H. Li, S. Yan, Surface-induced polymer crystallization and the resultant structures and morphologies. *Macromolecules* **44**, 417–428 (2011).
49. W. Shi, T. Zhao, J. Xi, D. Wang, Z. Shuai, Unravelling doping effects on PEDOT at the molecular level: From geometry to thermoelectric transport properties. *J. Am. Chem. Soc.* **137**, 12929–12938 (2015).
50. A. Weathers, Z. U. Khan, R. Brooke, D. Evans, M. T. Pettes, J. W. Andreasen, X. Crispin, L. Shi, Significant electronic thermal transport in the conducting polymer poly(3,4-ethylenedioxythiophene). *Adv. Mater.* **27**, 2101–2106 (2015).
51. H. Peng, N. Kioussis, D. A. Stewart, Anisotropic lattice thermal conductivity in chiral tellurium from first principles. *Appl. Phys. Lett.* **107**, 251904 (2015).
52. J. Callaway, Model for lattice thermal conductivity at low temperatures. *Phys. Rev.* **113**, 1046–1051 (1959).
53. M. Holland, Analysis of lattice thermal conductivity. *Phys. Rev.* **132**, 2461–2471 (1963).
54. A. Sahu, B. Russ, N. C. Su, J. D. Forster, P. Zhou, E. S. Cho, P. Ercius, N. E. Coates, R. A. Segalman, J. J. Urban, Bottom-up design of de novo thermoelectric hybrid materials using chalcogenide resurfacing. *J. Mater. Chem. A* **5**, 3346–3357 (2017).
55. S. Lin, W. Li, Z. Chen, J. Shen, B. Ge, Y. Pei, Tellurium as a high-performance elemental thermoelectric. *Nat. Commun.* **7**, 10287 (2016).

Acknowledgments: We thank J. Wu for allowing access to the probe station for nanowire manipulation. **Funding:** This work was partially performed at the Molecular Foundry, Lawrence Berkeley National Laboratory, and was supported by the Department of Energy, Office of Science, Office of Basic Energy Sciences, Scientific User Facilities Division of the U.S. Department of Energy under contract no. DE-AC02-05CH11231. M.P.G. acknowledges the NSF for fellowship support under the NSF Graduate Research Fellowship Program. A.K.M. acknowledges funding support from the ITRI-Rosenfeld Fellowship from the Energy Technologies Area at Lawrence Berkeley National Laboratory. **Author contributions:** L.Y. conducted thermoelectric property measurements and gate-modulated electrical conductivity measurements. L.Y., M.P.G., and A.K.M. performed thermoelectric modeling using the Kang-Snyder model. M.P.G. and K.H. synthesized Te-PEDOT:PSS and Te-PVP hybrid nanowires. A.B. and M.P.G. performed transmission electron microscopy characterizations. L.Y., M.P.G., and A.K.M. compiled and analyzed results. M.P.G., L.Y., J.J.U., and R.S.P. conceived and directed the project. L.Y., M.P.G., and A.K.M. wrote the manuscript with input from all authors. **Competing interests:** The authors declare that they have no competing interests. **Data and materials availability:** All data needed to evaluate the conclusions in the paper are present in the paper and/or the Supplementary Materials. Source data are available from the public repository (DOI: 10.5281/zenodo.4632461). Additional data related to this paper may be requested from the authors.

Submitted 1 September 2020
Accepted 24 March 2021
Published 14 May 2021
10.1126/sciadv.abe6000

Citation: L. Yang, M. P. Gordon, A. K. Menon, A. Bruefach, K. Haas, M. C. Scott, R. S. Prasher, J. J. Urban, Decoupling electron and phonon transport in single-nanowire hybrid materials for high-performance thermoelectrics. *Sci. Adv.* **7**, eabe6000 (2021).

Decoupling electron and phonon transport in single-nanowire hybrid materials for high-performance thermoelectrics

Lin Yang, Madeleine P. Gordon, Akanksha K. Menon, Alexandra Bruefach, Kyle Haas, M. C. Scott, Ravi S. Prasher and Jeffrey J. Urban

Sci Adv **7** (20), eabe6000.
DOI: 10.1126/sciadv.abe6000